CZECH TECHNICAL UNIVERSITY IN PRAGUE

Faculty of Electrical Engineering

Department of Telecommunication Engineering

Bachelor thesis

Fiber optic sensor for wind gust measurement

Prague
2014

Author: Jakub Maršálek
Supervisor: Ing. Bc. Leoš Boháč, Ph.D.

Čestné prohlášení: Prohlašuji, že jsem zadanou bakalářskou práci zpracoval sám s přispěním vedoucího práce a konzultanta a používal jsem pouze literaturu v práci uvedenou. Dále prohlašuji, že nemám námitek proti půjčování nebo zveřejňování mé bakalářské práce nebo její části se souhlasem katedry.

Affidavit: I hereby confirm that I prepared this thesis independently, by exclusive reliance on the literature and tools indicated therein. This thesis has not been submitted to any other examination authority in its current or altered form, and it has not been published.

Date 23. 5. 2014

.....

Student's signature

Acknowledgment

I would like to express thanks to Ing. Bc. Leoš Boháč, Ph.D. for his multiple feedbacks, as well as numerous consultations and weekend e-mail exchanges. His patient guidance and dedication to topics was irreplaceable and finishing the thesis would not be possible without it.

I also wish to thank Ing. Ladislav Šašek, CSc. , the director and executive of Safibra s.r.o, who made possible the whole concept of thesis to be physically realized instead of end up in library dust. I thank him for many advices and discussions over the countless tiny problems, as well as for chance to be part of the work on great projects.

Finally, would like to thank the Safibra project team Jaroslav Demuth, Robin Schilhart, Břetislav Bakala and Pavel Chára. They create an invaluable work environment, which increases motivation to continue the measurements and data processing, even in late nights hours.

Abstrakt

Tato bakalářská práce popisuje návrh a vývoj vláknově optického senzoru pro měření nárazů větru spolu se sadou testů, které definují technické parametry senzoru. Senzor byl sestaven pro použití v reálném prostředí a je schopen spolehlivého měření i v obtížných podmínkách, ve kterých standardní elektronické senzory mohou selhat. Pro výrobu byly použity běžně dostupné komponenty a technické parametry vyvinutého senzoru mohou být snadno změněny dle požadavků zákazníků. Tato práce obsahuje popis měření a výsledků, na jejichž základě je možné stanovit vlastnosti vyvinutého senzoru, jako je citlivost, stabilita nebo rozsah použití.

Klíčová slova: měření větru, braggovské mřížky, vláknová optika, optické senzory, teplotní kompenzace

Abstract

This bachelor thesis describes design and development of optical sensor for gust wind measurements, as well as set of tests defining its technical parameters. Sensor was built to be used in real environment. Sensor is capable of reliable measuring in different environmental conditions, which in the standard electronic sensors may fail. Sensor consists of commonly available components and its technical specifications can be easily changed reliant on customer needs. Thesis contains description of measurements and establishes the attributes of developed sensor such as sensitivity, stability or range of use as well. The realization process and consequent parameters are presented.

Index Terms: wind measurement, fiber bragg grating, fiber optics, optical sensor, thermal compensation

Contents

1 Introduction

Optical fibers are used in field of telecommunication, mainly for high speed data transfer. Its advantages involve strong immunity to electromagnetic field, data transfer security, elimination of electrical sparks and reliable applications over long distances as well as implementation in specific sensor applications [1]. Optical fiber technology can be used for measurement of various phenomena, for example temperature [2], mechanical stress, precise movement changing etc [3]. Nowadays, one of the most popular ways for such measurements is using FBG (fiber bragg grating).

Developed sensor is based on mechanical transfer of wind gust power into optical measuring system. Basic principle is at figure 1.1.

Figure 1.1: Basic principle

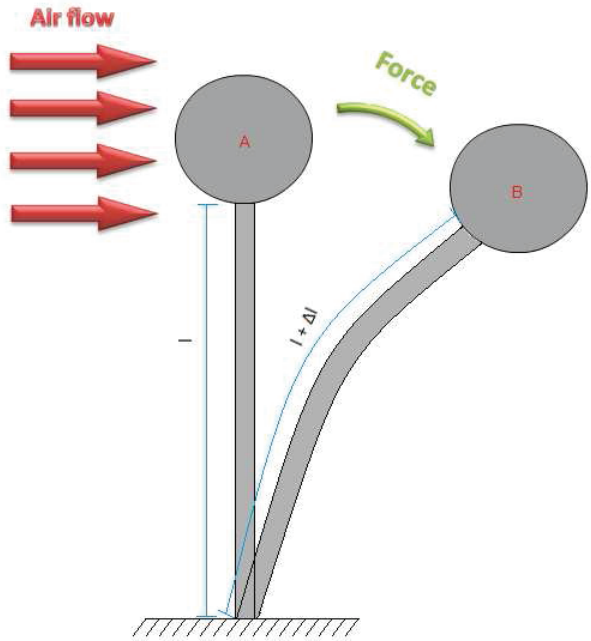

Sensor's movement from status (A) without an air flow to status (B). The force represents an effect of air flow towards the sensor. Dimension of sensor's body is marked l, while sensor is in status (A). Dimension of sensor's body can be expressed as $l + \Delta l$, while sensor is in status (B). The Δl represents an extension caused by mechanical bend.

In default condition without an air flow, the sensor stays in position (A). An additional wind gust creates a force pushing into the orb. This force leads to sensor bend, which is commensurable to power of the wind gust. According to technical theory of elasticity, sensor's length l is changed about length Δl.

Analytic establishment of Δl can be calculated by solving one of the basic mechanical role - the Cantilever. The cantilever scheme is at figure 1.2.

Figure 1.2: Cantilever scheme[22]

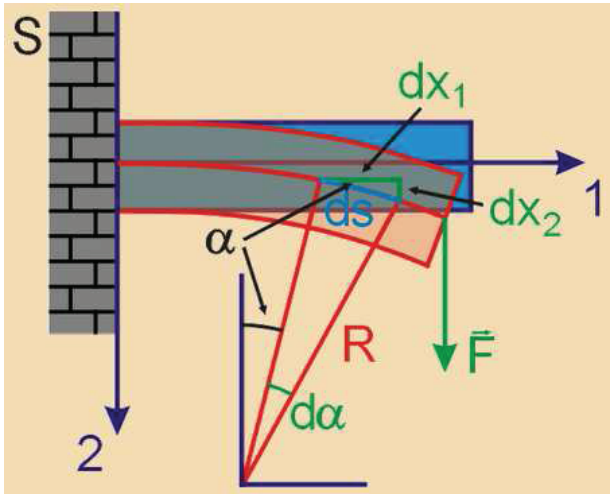

The (S) represents fixed part of reference system. Axes (1) and (2) denotes orientation of reference system.The dx_1, dx_2 and $d\alpha$ are infinitesimal length and angle, which defines basic space element ds. The (R) is a radius of characteristic circle and $\vec{F}$ is the bending force.

Equation 1.1 shows relations between coordinates $x_1$and x_2, elastic modulus E, quadratic section modulus $I_a$and force F. Force F bends the cantilever at distance l.

$$\frac{d^2x_2}{dx_1^2} = \frac{1}{EI_a}F\left(l - x_1\right) \tag{1.1}$$

Equation 1.2 is the result of several integrations. It shows a final mechanical extension in direction of axis (1). Standard definitions of elastic modulus and quadratic section modulus were used. The integration constants were established from cantilever scheme (figure 1.2)[1].

$$x_1 = \frac{Fl^3}{3EI_a} \tag{1.2}$$

The initial problem, the evaluation Δl from figure 1.1, is solved by substitution $x_1 = \Delta l$. TheΔl is commonly known as a mechanical stress.

[1]Precise analytic solution is in bibliography [22].

An FBG was used as measuring optical system. The FBG can evaluate Δl, if it is composed into mechanical construction correctly.

An exact understanding of electrodynamics and mechanics is not needed to comprehend this thesis. Precise illation of presented conclusions (the famous Maxwell's equations) will be skipped. The reader is assumed to have some knowledge over optical fiber technology.

The structure of developed sensor and used materials were chosen after careful consideration of parameters of the commercially used electronic sensors for gust wind measurements[2], as well as presumed need for precision, sensitivity and price of manufacturing[3]. The structure was designed for special applications rather than a serial production.

Presented sensor is subject to project GUARDSENSE (VG20102015053 - The modern structure of photonic sensors and new innovative principles for intrusion detection systems, integrity and protection of critical infrastructure)[4]. Final results, such as sensitivity, total dimensions, thermal stability, range of measurement or the mechanical resistance, will be presented along with methodology used in a depth that project confidentiality allows.

[2]Some of these sensors can be found at http://www.vaisala.com/en/products/windsensors/Pages/default.aspx

[3]Competitiveness of such device was the main concern, since many sensors for such measurements are already commonly used on different principles than fiber optics (fiber bragg grating in this case).

[4]Project itself has status of classified secret for commercial reason (according to par. 17-20 of Commercial Code), which prohibits to reveal all context and conclusions made during the development process. Details can be found at Research and Development and Innovation Information System of Czech Republic http://www.isvav.cz/projectDetail.do?rowId=VG20102015053

2 Mechanical draft - used components

The concept of developed sensor is shown at figure 2.1 below.

Figure 2.1: Sensor concept[4]

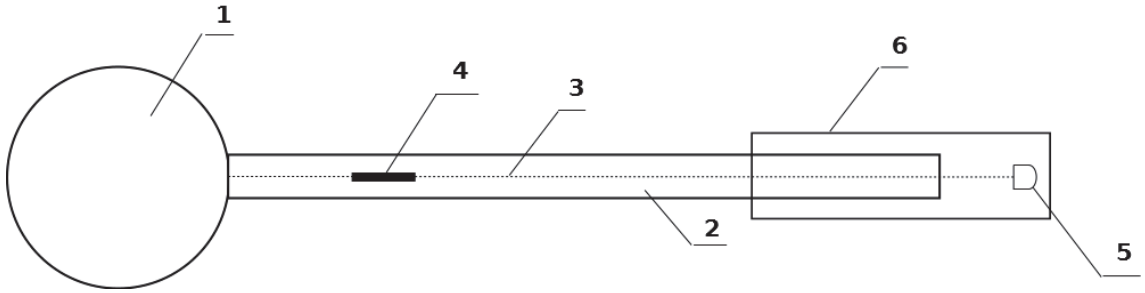

The special fiber with bragg grating structure in its core (4). This fiber (3) is placed in the middle of flexible tube (2) along its all length with both ends of the fiber fixed to the tube. Tube itself is ended with an orb (1), which is left in open environment and moves according to the wind gust. The opposite side of tube is fixed in the clamping structure (6). This clamping structure can be attached easily to the bridge, building or any other object where measurement of wind gust is required. One end of measuring fiber is connected to fiber optic connector (5), which allows to plug the sensor to evaluation unit such as spectrometer.

2.1 Optical fiber and FBG

In building process, the standard single mode telecommunication optical fiber SM9/125[1] was used. A FBG was "written" into this fiber. A central wavelength of FBG was chosen to be a 850nm[7.1]. Because of need for less expensive equipment for wavelength shift evaluation[2].

There are several ways to "write"[3] FBG to optical fiber. This specific technology reflects the final spectral characteristics of FBG (reflectivity and the spectral width for example) and its mechanical properties (such as the allowed mechanical elongation). Precision of periodic changes of refractive index is required if the high reflectivity and small spectral width is needed[5]. Standard procedure is to "write" the grating after whole drawing process and recoat[4] the exposed space after the process is done. The

[1]Where 9 refers to the diameter of fiber core and 125 to total the diameter of cladding in µm.

[2]Can be consulted at http://www.oceanoptics.com/Products/spectrometers.asp or any other seller.

[3]Bragg grating are made by periodical changes in refractive index of fiber core[5]. Usually, the modification in core are made by UV laser beam, which "writes" into fiber core.

[4]Coating[8] is primary protection of waveguide (core and cladding).

DTG grating[5] was used in this case, which denotes writing during the fiber drawing process. This technology leads to lower absolute power reflection of FBG grating, because of less precision of writing process. That is caused by movement speed of the fiber[6]. One of the biggest advantages is the higher mechanical strength. Since the sensor is supposed to be exposed to extreme environmental conditions, the mechanical properties were the main reason for choosing this technique. Other advantages and specifications of described technology are to be found in bibliography[7].

2.2 Orb and outer tube

The fiber is fixed inside the supple tube along its length. The tube is mechanically resistant enough not to be broken by higher wind gust. In this case, the special composite material was used. A rotationally symmetrical orb made of composite material is placed on the top of the tube's higher part. If bottom end of the sensor is immobile against blowing wind, upper orb is moving according to the force of the wind gust pushing into its surface in direct proportion. The diameter of used orb and the length of the tube are the main parameters of dynamical range of developed sensor [6].

2.3 Clamping structure and connector

The special clamping structure (annex 7.2) was used for establishment of the technical parameters. The most important thing was to ensure invariance of mechanical force along with the angle of tilt. That was achieved by precise circular holes in the body of clamping structure. Connector FC/APC[7] was used for low price and low typical loss[9].

[5]Drawn Tower Gratings
[6]Precise theoretical solution will be presented in section 3.
[7]Fiber connector - angled physical contact.

2.4 Final appearance

Final appearance of developed sensor is shown at figure 2.2. Dimensions of presented sensors are purposely not stated[8].

Figure 2.2: Final appearance of developed sensor

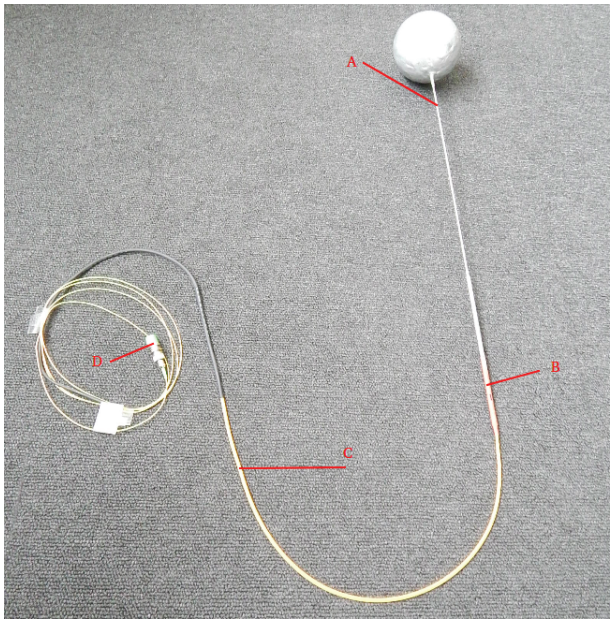

The (A) indicates body of developed sensor, (B) is area specifically designed to be closed into clamping structure, (C) is input optical cable and (D) FC/APC optical connector.

[8]Classified secret.

3 Theoretical background

In following part, some necessary physical connections and theoretical conclusions in field of electrodynamics will be described (especially the fiber optics and the theory of diffraction structure). A standard Newtonian mechanics (mechanical response of objects to force of wind gust in field of aerodynamics) will follow. Many approximations and omissions were made for better understanding of used principles and sensor development process[1] .

3.1 Diffraction structures and optical fiber

Optical fiber technology is based on total reflection[11] of injected light beam from one end to the other along its entire length. The reflection and refraction phenomena obeys the generic Snell's law. It is given by equation 3.1 in vector form and its commonly known scalar form is shown in equation 3.3. His graphic interpretation is shown at figure 3.1.

$$\begin{cases} (k_1' - k_1) \times \nu = & 0 \\ (k_2 - k_1) \times \nu = & 0 \end{cases} \tag{3.1}$$

$$k = \frac{2\pi}{\lambda} n_{eff} \tag{3.2}$$

Equation 3.2 shows relationship between wavevector k, wavelength λ and effective index of refraction n_{eff}.

$$n_1 sin(\theta_1) = n_2 sin(\theta_2) \tag{3.3}$$

[1]Here we talk about solution of Maxwell's equations, where the homogeneity, isotropy, linearity, low intensity of light, etc... are assumed. An isotropy of SiO_2 in used fiber and precision of period in diffraction structure (bragg grating) are assumed as well. The non-circularity response of used components was neglected also.

Figure 3.1: Snell's law[13]

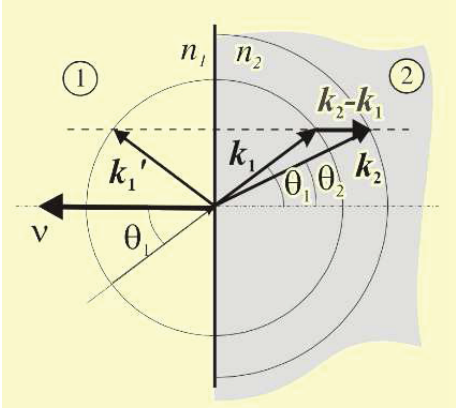

Here is the graphic solution of wave refraction in its vector form. The $n_1$and $n_2$are different refraction indexes of medium, k'_1, k_1, k_2,are appropriate wave vectors, andν is normal vector perpendicular to plane interface.

Critical angle $\theta_c$for total inner reflection is given by modification of equation 3.3 for $\theta_2 = 90°$.

$$\theta_c = \theta_1 = arcsin(\frac{n_2}{n_1}) \tag{3.4}$$

The critical angle of total reflection is 58,09° for used standard telecommunication fiber SMF-28e, considered the refraction index of coren_1= 1,46 and refraction index of cladding n_2=1,44 (for $\lambda = 1550nm$). Inner total reflection leads to signal's low attenuation on distances up to 100km[2].

The diffraction grating (special case of general diffraction structure which subsumes some kind of periodicity) such as bragg grating can be observed as basic periodically modulated interface. For solving the question of refraction on such interface, the Snell's law (appropriately modified for inner periodicity of some material constant such as refractive index) can be used in its vector form. The Snell's law must be fulfilled for estimated angular frequency of structure periodicity $K = 2\pi/\Lambda$, where Λ is the period of modulation. From phase relations between incident and refractive waves, the validity of equation 3.5 can be shown (where m is integer number).

$$(k_2 - k_1 - mK) \times \nu = 0 \tag{3.5}$$

Snell's law comes from dependence of tangential component of wave vectors[3]. The equation 3.5 can be labeled as grating equation, where K is grating vector pointing in

[2]Depends on exact type of fiber, power and wavelength of source, but for standard telecommunication optical fiber SMF-28e has normalized attenuation (source cat. C by ITU-T G.652) around 0,2dB/km[?]

[3]This can be estimated by examination of the Maxwell equations - boundary interface conditions [11]

the direction of gradient of modulation and ν is the unit vector in direction normal to the grating interface.

According to theory of diffraction, the diffracted waves creates a characteristic interference pattern (corresponding with grating parameters) after passage through the structure (and / or after reflection from it). Final field distribution in certain distance depends on phase shift of specific waves (each of them has its own wave vector and direction). The combination of partial contribution of every wave in each point in space (given specific coordinates) has the interference pattern as the result.

A bragg diffraction condition in general form (this can be derived from 3.5 for a plane wave using interference vector's definition[13]) is expressed by equation 3.6:

$$k_d = k_1 + K \tag{3.6}$$

Here, the$K$ is local interference vector describing the evolution of interference field, k_d is wave vector of diffracted wave and $k_1$is wave vector of incident wave. The K vector is perpendicular to interference plane (which is set of points, where interference pattern is stationary) and its size is inversely proportional to the space modulation period. In other way, satisfaction of this condition is required for constructive interference (combination of waves with right phase) of diffracted waves. Because wavelength is related to wave vector according to equation 3.2, relation 3.6 can be re-written to another form - the equation 3.7.

$$\frac{2\pi}{\lambda} n_{eff} + \frac{2\pi}{\Lambda} = -\frac{2\pi}{\lambda} n_{eff} \tag{3.7}$$

Now divide equation 3.7 by 2π and simplify. We get equation 3.8, where Λ is the period of grating and n_{eff} the effective index of refraction[12].

$$\lambda_B = 2 n_{eff} \Lambda \tag{3.8}$$

3.2 Fiber bragg grating

Fiber bragg gratings (FBG) are made by applying of bragg grating theory to optical fiber. That means creation of periodical changes in fiber core according to equations in section 3.1. Central bragg wavelength λ_B moves with change of mechanical grating period (for simplification is the refractive index taken as a constant for one grating)[4]. The resulting wavelength shift $\Delta\lambda$ is shown at figure 3.2.

[4]Directly concluded from equation 3.8.

Figure 3.2: Wavelength shift caused by change of grating period[14]

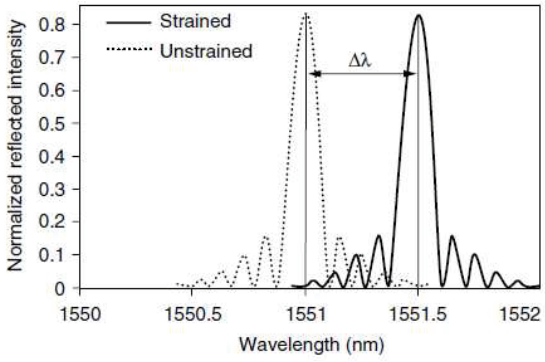

s

This figure exhibits the change of light spectrum caused by mechanical strain of FBG grating, which leads to alternation of grating period Λ.

Typical length of FBG in optical fiber is about 8mm. Figure 3.3 represents main properties of signal in spectral domain. The central wavelength of FBG has refracted only 80%, not all the energy in given spectral range[5].

Figure 3.3: FBG principle[15]

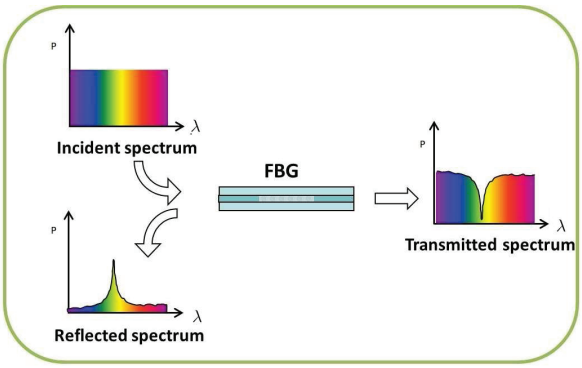

Whole spectrum of signal (Incident spectrum) is coupled into the fiber with FBG. A part of spectrum (the wavelengths fulfilled the bragg's condition given by equation3.8) is reflected back to the source (Reflected spectrum) when signal reaches the diffraction bragg grating. The remained part of the signal (wavelengths aside the bragg's condition) goes through the grating and continues in the fiber (Transmitted spectrum).

There is a simplified version of grating equation (derivable from equation 3.8) for fiber brag grating, which separates two main influences of wavelength shift - a mechanical

[5]Real characteristics of used FBG is attached in annex 7.1.

strain and a thermal expansion. A measurement of mechanical or thermal effects only is required for many application. Ts impossible to determine which effect, thermal or mechanical, was the source of the measured wavelength shift because the thermal status change has the mechanical expansion of material as a sight effect. Mathematical expression is shown in the equation 3.9[20]:

$$\frac{\delta\lambda}{\lambda_0} = (1 - p_e)\varepsilon + (\alpha + \xi)\Delta T + \eta\Delta P \tag{3.9}$$

where p_e , α, ξ , and η represent the effective photoelastic, attenuative, thermo-optic, and Young's modulus coefficients of the fiber material, respectively ε, T, and P denotes the strain, temperature, and pressure changes. The pressure is constant for most application, which means the $\Delta P = 0$. Standard procedure for temperature compensation is to use multiple FBGs and place them away from supposed measurement point of mechanical stress, yet close enough to experience the same thermal fluctuation. The status of both FBGs can be reformulated into matrix form as an equation 3.10[21], using equation 3.9.

$$\begin{pmatrix} \Delta\lambda_1 \\ \Delta\lambda_2 \end{pmatrix} = \begin{pmatrix} K_{1\varepsilon} & K_{1T} \\ K_{2\varepsilon} & K_{2T} \end{pmatrix} \begin{pmatrix} \Delta\varepsilon \\ \Delta T \end{pmatrix} \tag{3.10}$$

The K is parameter (obtaining constants in equation 3.9), indexes 1 and 2 indicates number of FBG, ε and T denotes the strain and temperature, and $\Delta\lambda$ the appropriate wavelength shift. Fixing one parameter K_{xy} leads to direct possibility to evaluate the accurate value of second - indifferent thermal or mechanical - through $\Delta\lambda$.

3.3 Mechanical properties of orb

It is possible to calculate mechanical response[6] of object exposed to some fluid (wind in this case) for given object's shape and size. This constant, describing such response, is a drag coefficient. It is a parameter used to quantify resistance of object in the fluid. Something about the validity of used computation methods and approximations needs to be said:

- An air in its standard condition is to be a Newtonian Fluid.[7]
- An approximations are valid for small speeds - down to 30m/s[8]

Dependence of the Drag coefficient on Raynolds number[18] is shown in figure 3.4, where Raynolds number is dimensionless numerical value, which represents similarity in flow patterns. It is defined according to equation 3.11, where R_e $[-]$ is Raynolds number, v $[m \cdot s^{-1}]$ is speed of fluid, D $[m]$ is characteristic diameter for a circular shape and ν $[m^2 \cdot s^{-1}]$ stands for the kinematic viscosity. The R_e represents proportion between an inertia force and an friction force by another physical interpretation. The Raynolds number is considered to be in order 10^5 for given wind speeds.

$$R_e = \frac{vD}{\upsilon} \tag{3.11}$$

[6] A general reverse force from object to fluid.
[7] This comes from relations around the dynamic viscosity, kinematic viscosity and density[18]
[8] A tornado according to Beaufort scale

Figure 3.4: Dependence of Drag coefficient on Raynolds number[17]

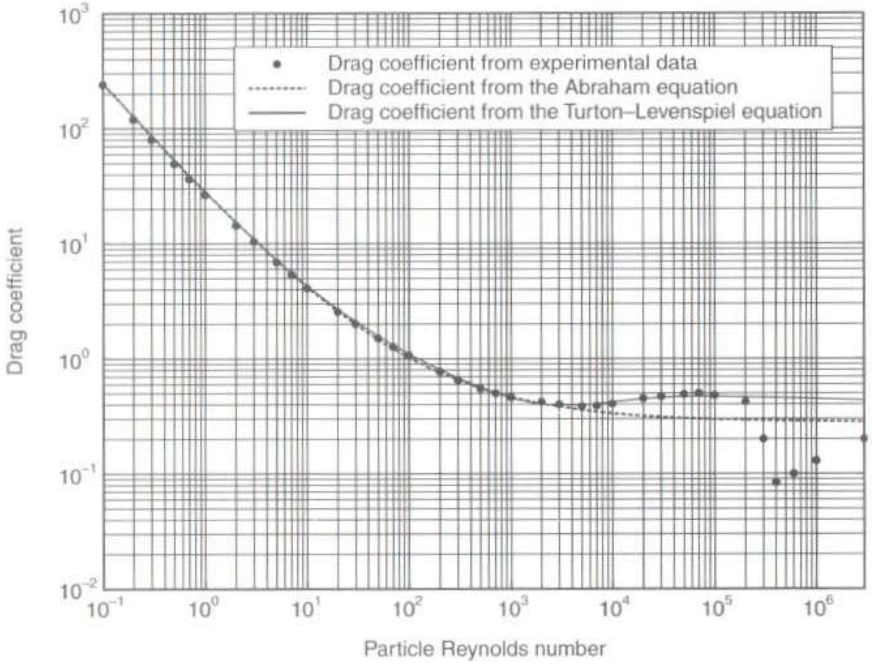

If is more precise to use a Stokes's drag law (left part of figure) describing the laminar regime, a modified Stoke's drag law (middle part of figure) describing the transition region or a Newton's drag law (right part of figure) describing the turbulent flow, is decided by position of the Raynolds number in figure 3.4 [9].

The resistance (drag force) of object surrounding by fluid is given according to following equation 3.12[17], through foregoing assumptions:

$$F = \frac{1}{2} C \rho S v^2 \tag{3.12}$$

where F $[N]$ is a drag force, C $[-]$ is a drag coefficient (coefficient of resistance for given shape), ρ $[kg \cdot m^{-3}]$ is density of the surrounding fluid and v $[m \cdot s^{-1}]$ is speed of the surrounding fluid.

Symbols and units used in calculations are shown in Table 3.1. The values are valid for standard atmospheric pressure and temperature 80°F[16]. Since the shape of sensor's active part is considered to be a perfect sphere, the numerical value for coefficient of resistance is 0,5. The surface of orb is taken as the only valid surface. The surface of tube is neglected for any numerical calculation in relation to global drag coefficient. Speed of air is measured through mechanical response of drag force F, which is evaluated form the spectral wavelength shift on the diffraction grating structure (FBG).

[9] The theory around differences of given regions is to be seen in bibliography [17, 18, 19].

Table 3.1: Used coefficients and values

Physical quantity	symbol	value	SI units
Drag coefficient	C	0,5	-
Density of air	ρ	1,17	$kg \cdot m^{-3}$
Drag area[10]	S	$2\pi R$	m^2
Speed of fluid	v	variable	$m \cdot s$

The presented theoretical part made the background for estimation of possible force effect. Using this equations is possible to approximately determine the relations between real wind flow and wavelength shift of light. Please, see the bibliography for deeper understanding at the end of thesis.

4 Sensor testing and evaluation

The main concern of every sensor are the terms of its use. The first step for choosing the right sensor is usually defining the application. In other words, we need to know what to measure, where to measure, and what results we expect to get back from measuring setup. The selection of function setup is based on sensors parameters. Parameters such as sensitivity, stability (thermal, mechanical or other), method of measuring and evaluation of data, precision of measured information and not less importantly the price of whole setup can be compared with previous expectations. The task was completed successfully when the results are balanced.

The set of experiments and measurements was made to define the most important parameters of developed sensor. Main purpose of the sensor is to measure high wind gust in conjunction to protect critical infrastructures[1]. It was specially designed to work with several other systems and methods[2]. The range of use, which depends on its parameters, was subordinated to needs of GUARDSENSE project. The intention was not to developed an almighty sensor with great precision or or sensor with large scope of applications but to find minimal level for sensor to work at, using as less resources as possible. Secondary intention was to figure out the dependences between attributes of used parts, to evaluate their influence and to find general possibilities of manufacturing, considering price and feature application needs. The testing was part of development process and tested sensor prototype was not intended to be having an ideal characteristics. More importantly, it was built to bring up more understanding of the topic, which was successfully done.

Unfortunately, the sensitive nature of the project prohibites all circumstances and conclusions from exposure. Some logical steps will stay hidden and many things will be presented as an axioms without correct proof. The following numbers and graphs are deliberately changed.Yet, the progression and shape of sensors functions are preserved but all numerical values has been normalized.

To determine necessary parameters, following set of measurements was made:

- Laboratory test of rotation symmetry
  - absolute distance
  - force response
- Laboratory test of linearity
  - absolute distance
  - force response
- Outside testing of linear response in given direction[3]
- Long-term outside testing in real environment

[1] As this thesis is sight result of work on GUARDSENSE Project.
[2] Which cannot be presented towards classified nature of the project.
[3] Since the sensor's response was found to be direction dependent.

Part about linearity and symmetry tests ("absolute distance test" and "force response test") was made for ascertainment, whenever possible nonlinearity or asymmetry has its origin in the physical nature of sensor's bending (since it's basic structure is not designed to be linear) or in the mechanical transfer of outer events to the detection FBG grating inside.

All of the tests were prepared with intention to evaluate more of dependencies (the circular function and rotation symmetry) and approximations rather then a precise set of numbers or sensor calibrations. All results will be commented below.

4.1 Laboratory tests

The measurements for evaluation of basic attributes (linearity, range, and rotation symmetry) were made on several laboratory setups. All points of interest were measured repeatedly to reduce the effect of measurement error (given by measuring method or precision of used devices). Final numbers are stated as an arithmetical average of measured points. Data used to evaluate the result of every laboratory test are summarized in annex 7.5 together with maximal value of statistical variance of each set. Basic background of testing method at figure 4.1.

Figure 4.1: Basic conception of testing method

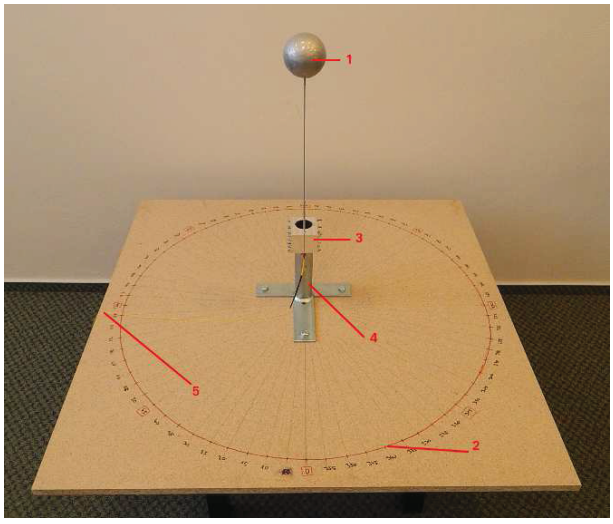

Basic concept consists from testing sensor (1) attached with clamping structure (3) to standard satellite antenna holder (4). The holder is screwed to a wooden table with marked angular scale. Signal from tested sensor is delivered to evaluation unit through optical fiber cable (5).

Every measured point was measured from zero position (sensor was not bend at all) directly to position, which was to be measured. For example, the distance from 0cm up to 5cm was measured on one movement in case of linear absolute distance for point correspond to 5cm. Every mesurement has been made three times.

4.1.1 Rotation symmetry of developed sensor

There direction dependence of sensor response during construction was observed. Understanding the nature of this phenomenon is critical for feature application, since the sensor was believed to measure in an open space (and dysfunction in one or more directions might significantly compromise it's utility).

Several measurements of sensor response to different kind of mechanical stress were made. All of them was made around whole circle with angular step 5°. Their setup is shown at following figures:

Figure 4.2: Small coil used in the rotation symmetry measurements

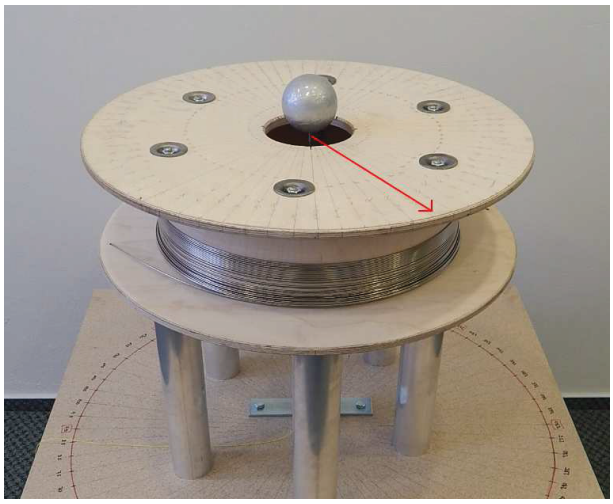

Inner diameter of presented small coil is 13,8cm. There is the same angular scale as on the wooden table below as at the surface of the small coil. Both scales are oriented at the same angles and directions. The scales are identical in case of right setup positioning.

Figure 4.3: Big coil used in rotation symmetry measurements

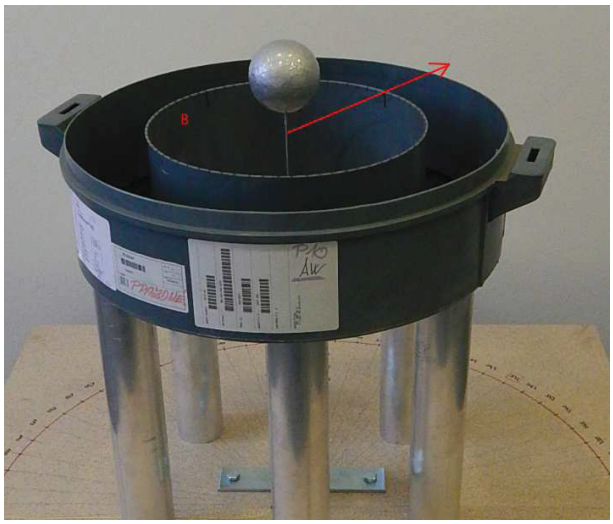

Inner diameter of presented small coil is 32cm. There is the same angular scale as on the wooden table below as at the surface of the small coil. Both scales are oriented at the same angles and directions.

Sensor was bent several times in every direction according to the angular scale spacing 5°. The inner edge of coils was used as a break point in case of absolute distance measurements. For establishment of force response, a standard dynamometer[4] was used. A dynamometer was attached to sensor, which was subsequently bent until the response of dynamometer reached out the required value. The resulting data were graphically processed and a set of values were assigned to every angular direction. From those, an arithmetical average and statistical variation[5] were established. Results will be discussed hereafter.

4.1.2 Linearity of developed sensor

Smoothness and monotony of the sensor functions are huge advantages for processing facilitation of the sensor response. It is easy to calculate any point on given curve (the line in this case) when characteristic functions (mechanical transfers into fiber) are linear.

The relation between mechanical stress effects to optical fiber and FBG grating is linear by definition[6]. Yet, the methodology of manufacturing must be considered. After that is clear (considering used parts and their mechanical attributes), the sensor does not have to have linear response to wind gust (spectral response of FBG is not linear according to linear force excitation to upper orb). From measurements of rotation symmetry was the angular dependence obvious. All linearity measurements were made

[4]Illustrative picture is in annex 7.3
[5]Changed source data can be seen in annexes (annex 7.5)
[6]Can be found in chapter 3 - Theoretical background

in four basic directions for comparison - 0°, 90°, 180° and 270° (to ensure the results validity all around the circle).

Figure 4.4: Setup used for linearity measurements - force response

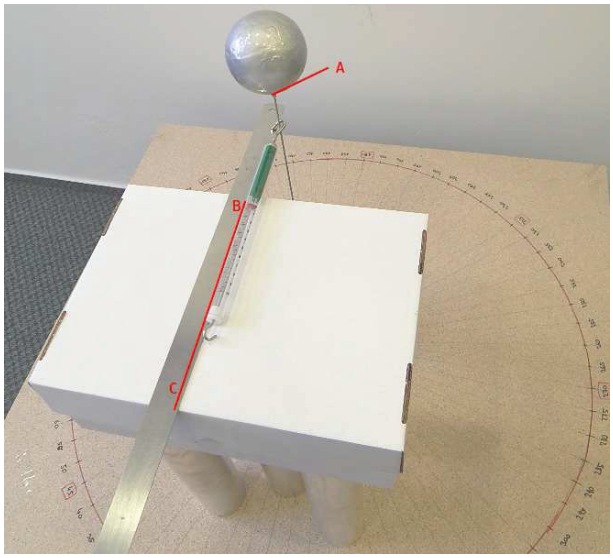

Points (A), (B) and (C) lies on one line. (A) is placed in the central axis of measured sensor, points (B) and (C) determine movement direction of used dynamometer. This direction was chosen to copy the distinguish tack of measured angles (0°, 90°, 180°,270°). Dynamometer's movement was bounded with bending of the sensor, causing appropriate sensor response.

At figure 4.4,the measurement setup for 0° direction is shown. The number of measured points was chosen according to previous calculation. The force pull went from 0,5N to 3N, with 0,5N step. It was impossible to ensure equally precise dynamometer pull to evoke smaller force response than 0,5N. Precision of used dynamomter was 0,1N[7].

[7]Precision of used dynamometer can be found at http://www.helago-cz.cz/product/presny-silomer-zeleny-10-n/

Figure 4.5: Setup used for linearity measurements - absolute distance

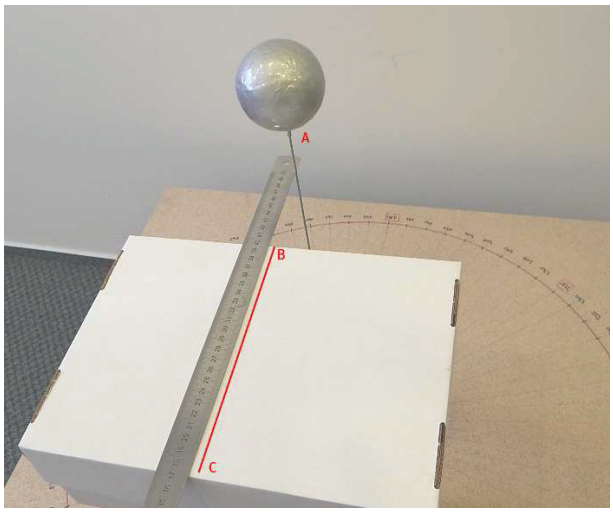

Points (A), (B) and (C) lies on one line. (A) is placed in the middle axis of measured sensor, points (B) and (C) determine movement direction of used dynamometer. This direction was chosen to copy the distinguish tack of measured angles (0°, 90°, 180°,270°). Dynamometer's movement was bounded with bending of the sensor, which causes the appropriate sensor response.

At figure 4.5, the measurement setup for 0° line is shown. The number of measured points was chosen according to previous force measurements to distances from 0cm up to 13cm with, 1cm step. Same setup was used for all four directions. The point (A) followed course of the red line [8] and sensor response was deducted in right distances.

A slight difference between measuring of absolute distance with coils (two different diameters, which bounds distance) and linear measurement (figure 4.5) must be accentuated. Method of linearity measurements was slightly different in angle and point of attachment. That leads to change of absolute values of the sensor response, together with inner sensor structure. Results will be discussed hereafter.

4.2 Outside measurements

The set of outside measurements in real environmental conditions to confirm the presumptions concluded from laboratory testing were made. An influence establishment of surrounding environment to previous results was first of them. Some of the complications of real environment are actual wind gust and turbulences, that could be much faster than real sensor response[9]. Another problem is small oscillation of sensor, be-

[8] Line from point (B) to point (C).

[9] It is ment the time the sensor needs to bend according to force of floating air, not the time sensor needs to measure and "send" some data. "Sending data" is done in speed of light, since the measuring element is diffraction structure and evaluation unit works with spectral characteristic of incoming light.

cause the sensor reacts to every wind gust by its characteristics step-response. Every step-response has its own time constant. The biggest issue to solve was the thermal instability (usually coming from sunshine). In Chapter 2 - Theoretical background, one way how to calculate accurate value of mechanical stress in an environment with changing temperature was already mentioned. Yet, this solution requires another measuring FBG grating which appeared to be inconvenient. A way to reduce effect of thermal instability under needed limits after additional testing was found.

4.2.1 Car roof - real linearity test

Sensor's response to both - small and high wind force needed to be tested. It is difficult to evoke wind flow in speeds around 30 m/s in laboratory conditions, so as the measuring setup the sensor attached to a car roof was used. Measuring setup is shown at figure 4.6.

Figure 4.6: Car roof - linearity test

Measuring sensor (A) is fixed with clamping structure (B) and attached to the roof sight side. The signal is transfered through optical fiber (C) to the evaluation unit placed inside of the car.

With this setup, the curve describing characteristic response of sensor in high wind speed as well as in low ones was measured.An air-screw anemometer (annex 7.4) was used as a reference. As car was moving in needed speeds, and responses of measured sensor were written down along with values on reference anemometer. Relevant values were enumerated from graphical signal and processed. Unlike laboratory tests, no statistical methods to lower impact from measurement inaccuracy (there was only one value for each point) were used. Results will be discussed hereafter.

4.2.2 Long-term outside testing in real environment

Developed sensor was put into outside real environment as a final measurement. Main cause of a long-term testing was to authenticate results from laboratory and and compared them to short-term testing setups. Also, a demand for higher thermal stability of developed sensor went out from this measurement. At figure 4.7, photo of installed sensor and reference anemometer GIOM 3000[10] is shown.

Figure 4.7: Installation of developed sensor in real environment

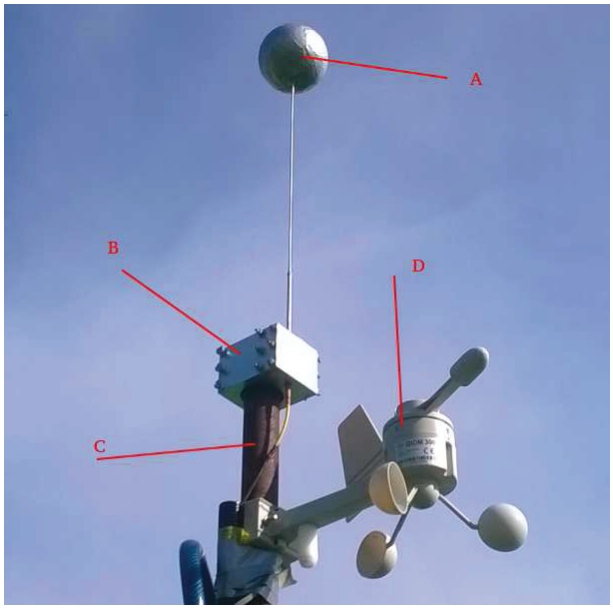

You can see measurement setup of installation. (A) is developed sensor fixes with clamping structure (B) to an iron tube (C). Reference anemometer GIOM 3000 is placed right below (D).

Results will be discussed hereafter.

[10]Details can be found at http://www.mikrovlny.cz/cz/produkt/57

5 Results of the measurements

In following part, the graphs of measured data are displayed. All the y-axis (usually "sensor response [au]) has been purposely changed[1] although the shapes of the result functions remained correct. Data are normalized to one reference value. This value is the same for all measurements, so it is to be seen as percentage efficacy for easier orientation. Many conclusions in this part are based on knowledge of the manufacturing process of developed sensor. Unfortunately, this process cannot be revealed.

5.1 Rotation symmetry of developed sensor

Graph of data from part 4.1.1 is pictured at figure 5.1.

Figure 5.1: Rotation symmetry - absolute distance

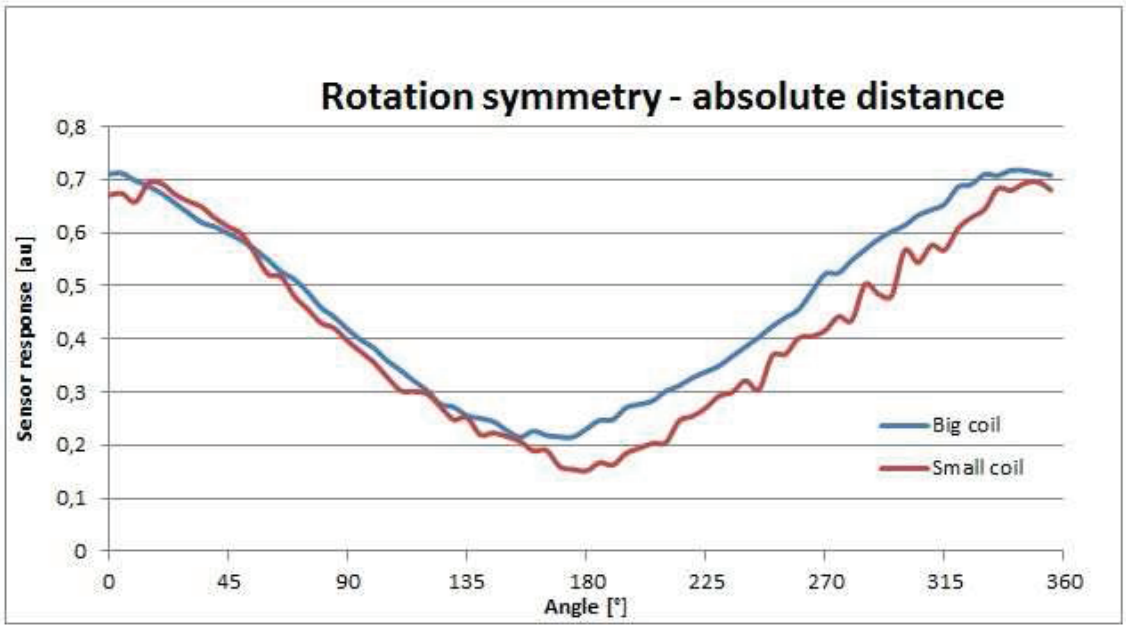

Dependence of sensor response on angle of bending. The absolute dimension of big coil is 32cm in diameter (upper blue), the small coil is 13,8cm in diameter (bottom red).

Two curves corresponding with two measurements are shown. They are depicted in one graph for clarity and easier comparison. The small coil had 13,8cm in diameter

[1] Classified secret for commercial reason (according to par. 17-20 of Commercial Code).

and the big coil 32cm. A twice bigger sensor response for a big coil was to be expected, yet the difference is almost negligible. The reason is hidden after the saturation of sensor (which is placed around value of 0,7au). It will be clearly seen in section "test in real environment". The shape of curves is given by inner sensor construction[2] and it was designed to look this way. Let's accentuate striking axis symmetry around 180°. The corrugation of curves is a side effect caused by used measurement method. The circular functions are shown at figure 5.2 below.

Figure 5.2: Rotation symmetry - circular function

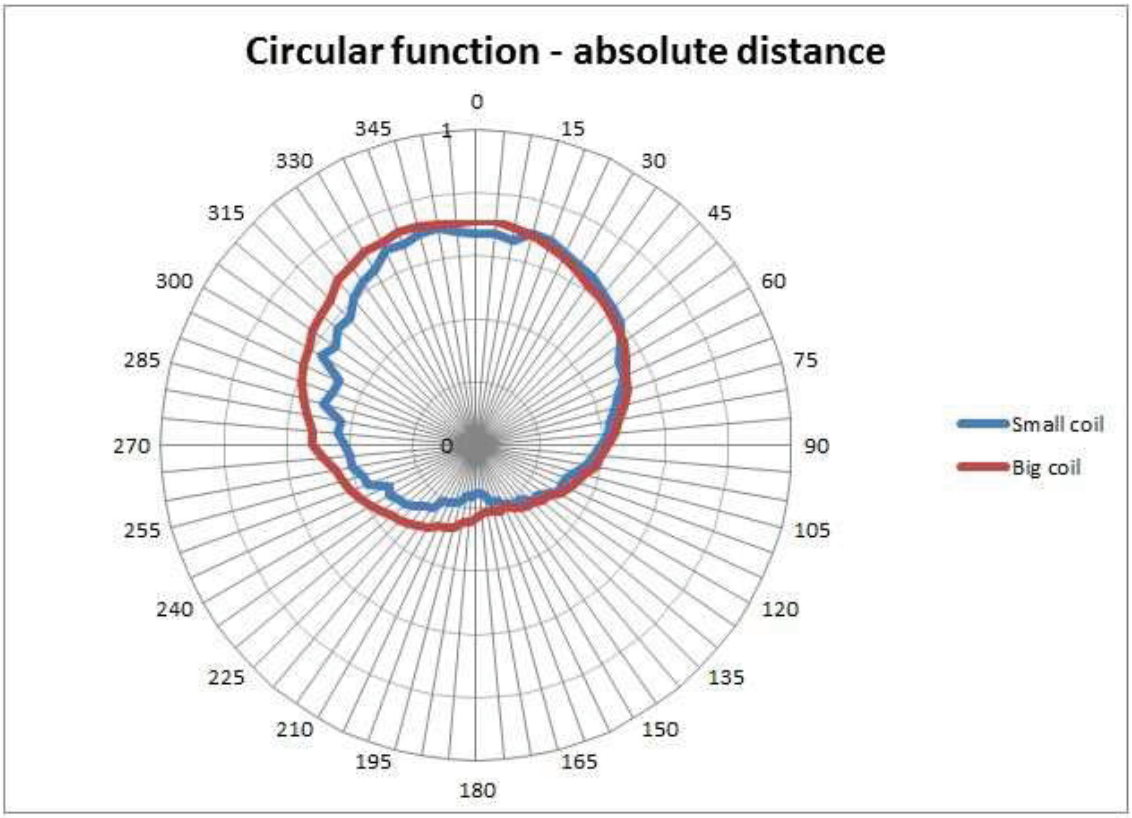

Circular function of developed sensor. This is how the sensor response looks like, placed in the middle (point 0) of scale and bend to same distance all around the circle.

The force dependent rotation symmetry was established through measuring setup described in part 4.1, using dynamometer as bending tool. Results are shown at figure 5.3.

[2]Classified secret.

Figure 5.3: Rotation symmetry - force response

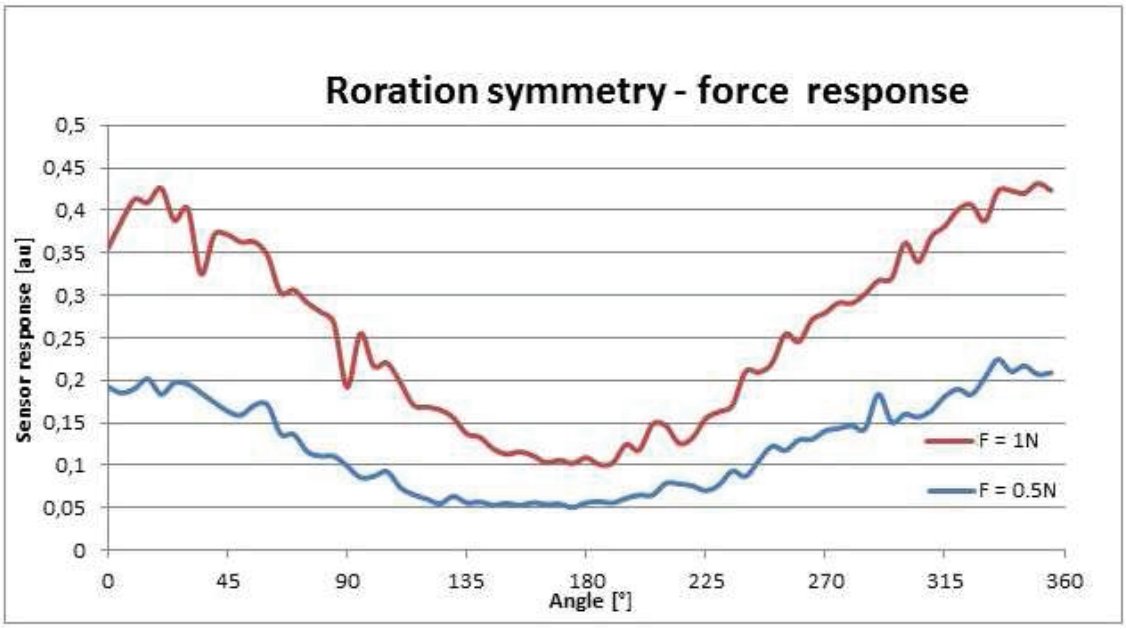

Dependence of sensor response on angle of bending. The force response is 0,5N (bottom blue) and 1N (upper red).

In this case, the sensor's respond for constant bending force 1N is about twice the value of curve belonging to force 0,5N. Cause of this difference against the first measurements - the absolute distance, is lower total percentage efficiency (lower sensor bend[3]) - which is below saturation threshold. Since measured sensor is the same, the shape of curve, given by inner sensor construction[4], is the same as before. Corrugation of curves is a side effect of the measurement method and the inaccuracy of used dynamometer. Similar circular function is shown at figure 5.4 below.

[3]Here is sensor response at 40% of maximum despite of 70% for measurement of absolute distance.
[4]Classified secret

Figure 5.4: Circular function - force response

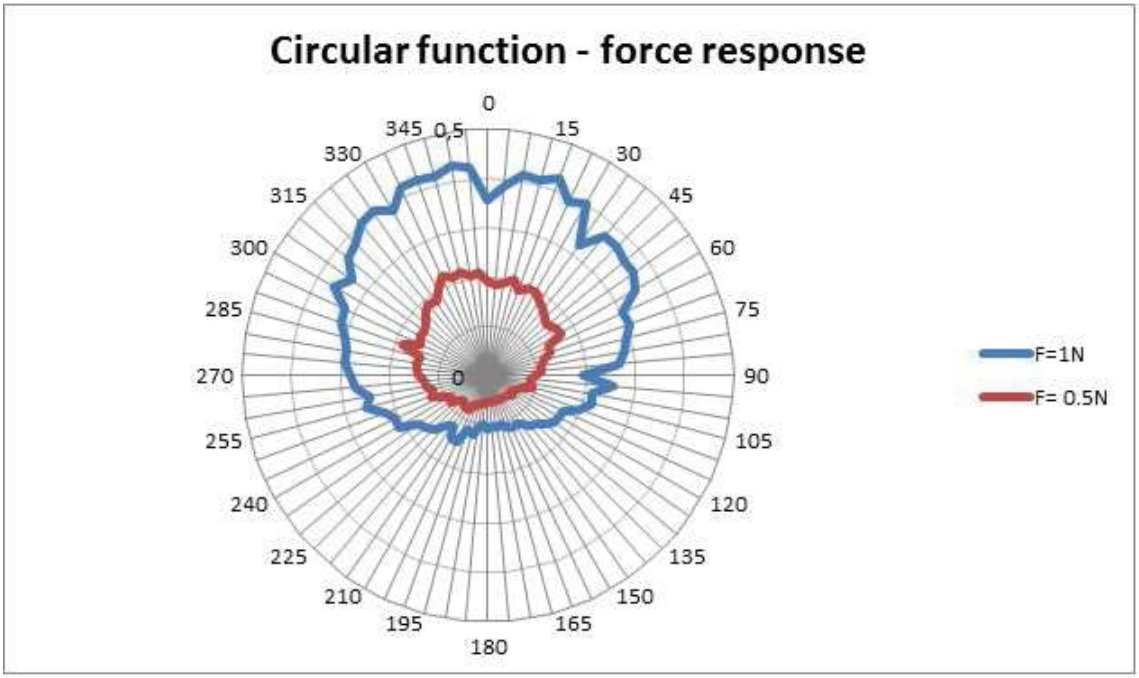

Circular function or directional characteristic of developed sensor.This is how the sensor response looks like, placed in the middle (point 0) of scale and bend with same force all around the circle.

5.2 Linearity of developed sensor

As stated before, the linearity comes with many advantages for feature data processing. Two kinds of measurements - linearity of bend in absolute distance (figure 5.5) and linearity of bend in absolute force were made. More information is in part 4.1.2.

Figure 5.5: Linearity - absolute distance

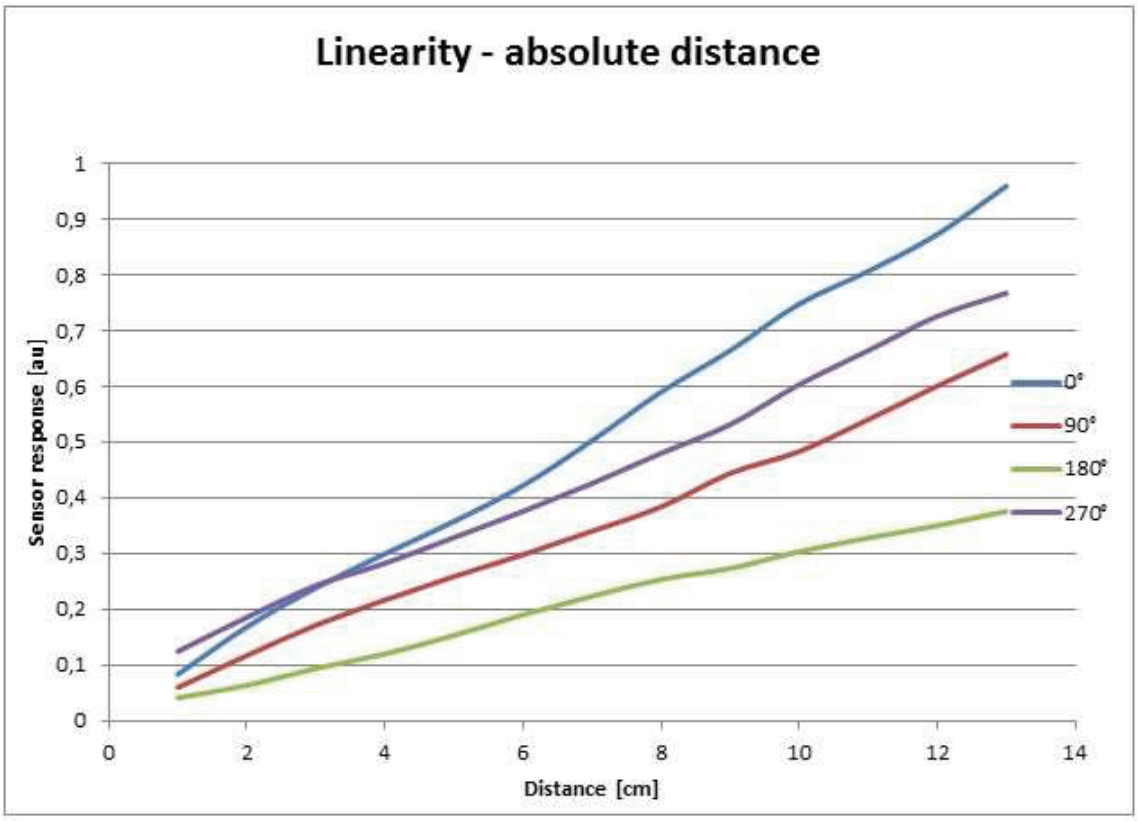

Graph presents dependence of sensor response in absolute distance from the center (point 0). Every curve belongs to one characteristic direction, labeled with its angle coordination.

All curves are linear, which indicates to fact the transmission from outer mechanical structure to detection FBG is also linear. The method of linearity measurements was slightly different in angle and point of attachment to the sensor's body. Together with inner sensor structure, it leads to change of absolute values of the sensor response. For this graphs (figures 5.5 and 5.6),the values in y-axis ("Sensor response [au]") are not comparable with rest of the data. The normalization effected maximum of sensor's response, which could lead to false conclusion that the sensor is measuring over the saturation and 100%). The important thing over presented curves is their shape.

Figure 5.6: Linearity - force response

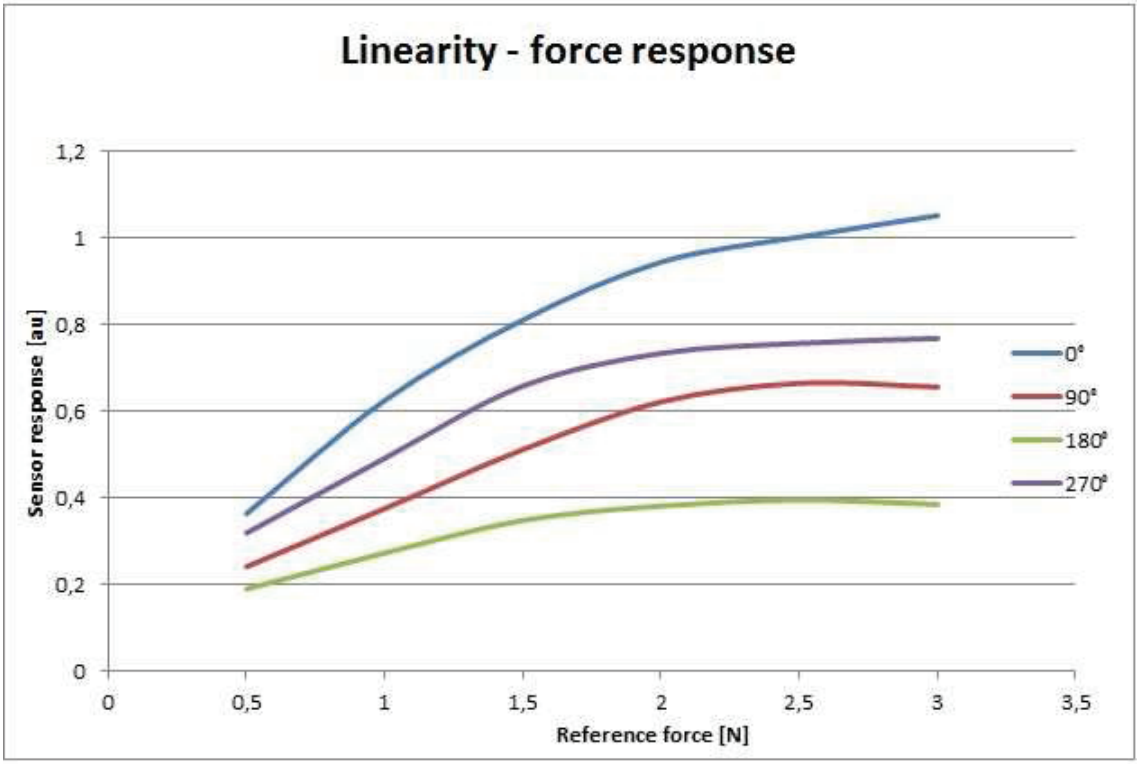

Graph presents dependence of sensor response to variable force stress. Every curve belongs to one characteristic direction labeled with its angle coordination.

At figure 5.6 the relation between sensor's response over the sensor bending is shown. Bending goes with linear change of the source power from 0,5N up to 3N, with 0,5N step. Despite of linear force bending, shape of the curves are cranked, which suggest the existence of maximum sensor response. That is no surprise since is impossible to bend sensor more than some certain limit given by attributes of used construction materials. This maximum response given by variable stiffness of sensor establishes sensor's saturation. Taken from the other side, the saturation encloses maximum force which the sensor is able to process correctly. Maximum force leads directly to maximum speed of wind gust.

5.3 Outside testing of developed sensor

Developed sensor was attached to the car roof as described in part 4.2.1.

Figure 5.7: Car roof - response test

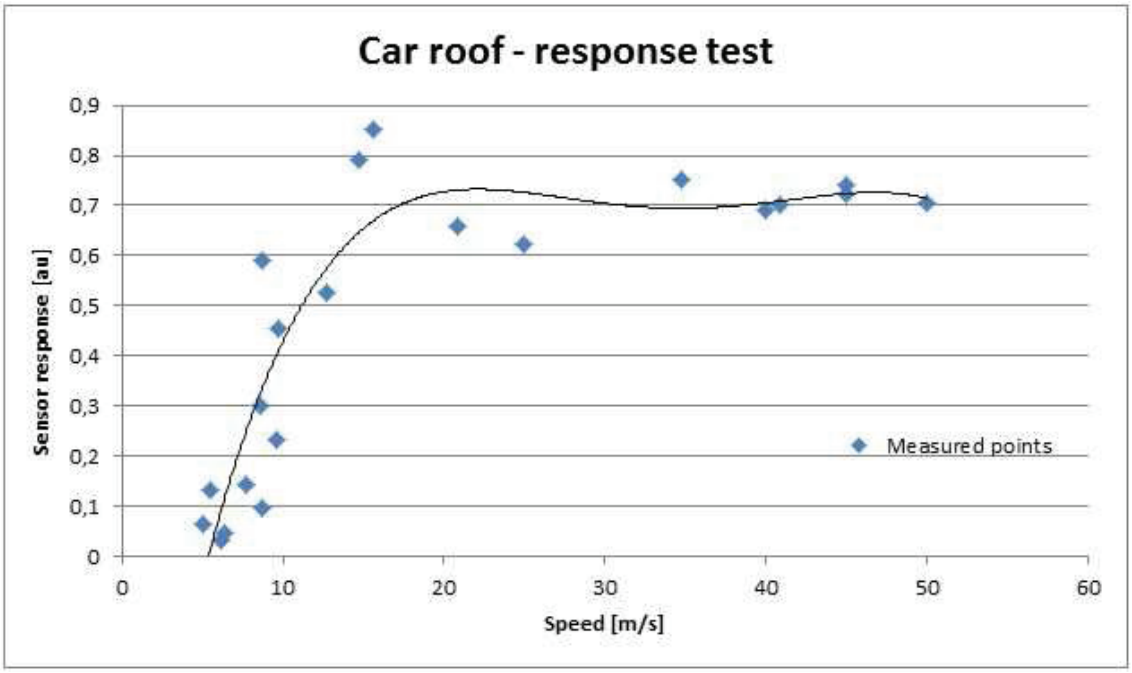

Dependence of sensor response on speed of surrounding air. The black curve marks data interlard by fourth degree polynomial.

Results from test in real environment can be viewed in graph on figure 5.7. There is the same saturation value as in previous measurements (around 0,7au). The change in sensor's response is neglectable over this value (matching the speed little over 20m/s). The curve is shifted for growing measuring defect in the part of lower air speed. This defect was caused by instability of the surrounding air and by road inequality transferred into sensor's movement.

5.4 Long-term outside testing in real environment

Developed sensor has been installed into real environment for long-term measuring. A commercially manufactured anemometer GIOM 3000[5] was used as thermal and wind speed reference. Data given by this device was compared with response of developed sensor. Commented results are about to be presented. There are several common facts which need to be taken under consideration.

Used reference anemometer is designed for a long therm measurement and speed of measuring is about 1 sample per minute, with build-in averaging. Developed FBG sensor is measuring real time with current sampling period about 100ms[6].

There exists a data loss and slight data corruption, which is caused by data processing inside of the evaluation unit (high peaks in red sensor response signal).

Next three graphs (figure 5.8, 5.9 and 5.10) were extracted from evaluation unit, which was used to measure sensor's response all along through whole testing process. The time sample is the constant. Difference between three red signals is caused by used processing and evaluating algorithm. That means, the outside conditions of surrounding environment were exactly the same for all the events shown on all three graphs.

Figure 5.8: Sensor response and wind speed

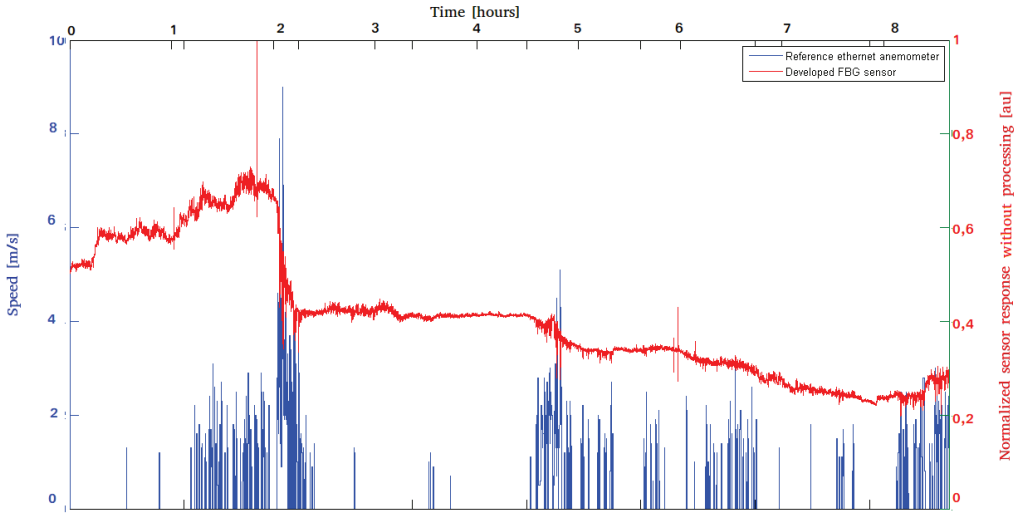

Values of developed FBG sensor are normalized (not to same size as in graphs before). The x-axis stands for time in hours, left axis for wind speed measured with reference anemometer GIOM 3000.

Comparison of reference wind speed signal (blue) with sensor response (red) is shown at figure 5.8. Red signal is extremely unstable without any apparent cause. Because the sensor is only able to measure absolute values of wavelength shift, establishment

[5]Details can be found at http://www.mikrovlny.cz/cz/produkt/57 and datasheet in annexes
[6]Sampling period is given by speed of evaluation unit, not by sensor.

of absolute value directly linked to wind speed deviation is next to impossible under these conditions.

Figure 5.9: Sensor respond and outside temperature

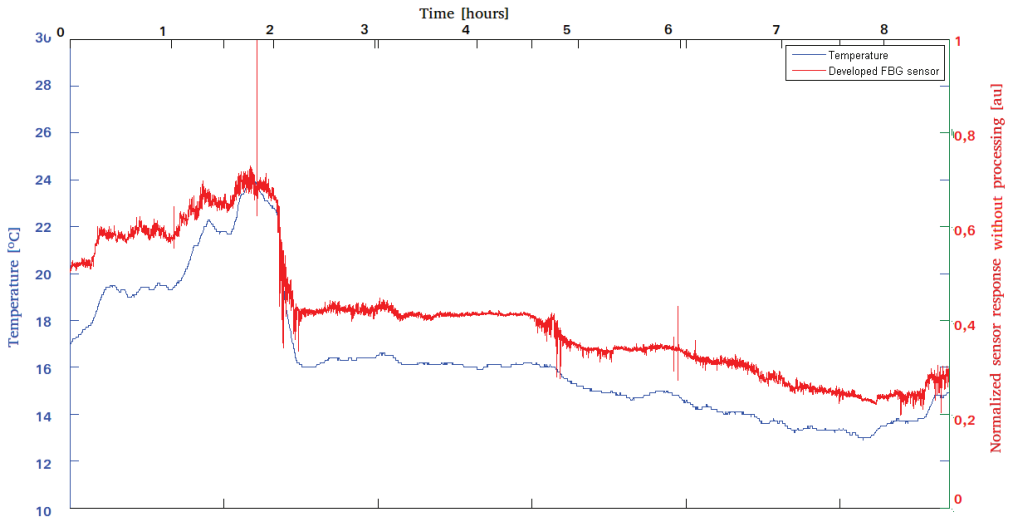

Values of developed FBG sensor are normalized. The x-axis stands for time in hours, left axis for outside temperature measured with reference anemometer GIOM 3000.

At figure5.9, the comparison of the outside temperature signal (blue) with sensor response (red) is presented. The dependency of changes in thermal status of surrounding air and shape of envelope curve is apparent from similarity between both signals. The physical essence of this phenomenon is described in chapter 3 and it directly certifies validity of bond between wavelength shift caused by the thermal extension and the one caused by mechanical stress, according to equations 3.9 and 3.10.

The results showen at figure 5.10 were achieved by right adjustment of processing algorithm in evaluation unit, which can not be reveled[7].

[7]Classified secret

Figure 5.10: Processed sensor respond and wind speed

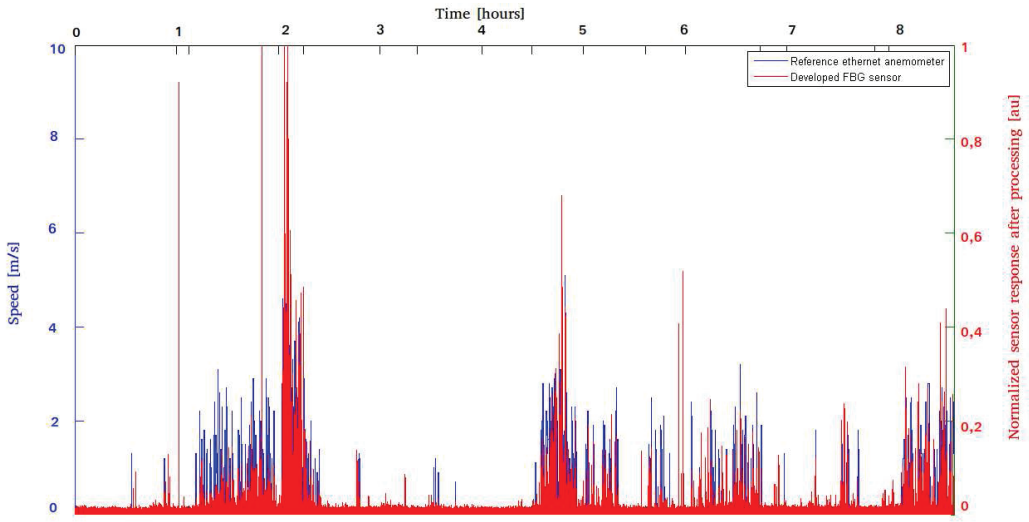

The blue signal represents the reference wind speed. The red signal represents normalized sensor response. The x-axis stands for time in hours, left axis for wind speed measured with reference anemometer GIOM 3000.

Red signal from developed sensor contains high similarity with reference measurements. Thin high peaks in red signal are faults coming from data corruption, based in evaluation unit.

Zoomed part of signal after data processing is shown at figure 5.11.

Figure 5.11: Processed sensor respond and wind speed - zoom

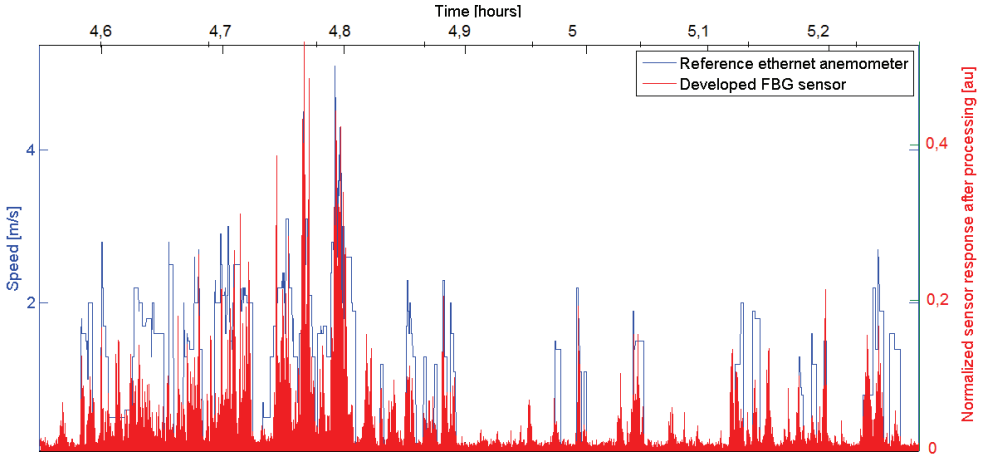

The blue signal represents the reference wind speed. The red signal represents normalized sensor response. The x-axis stands for time in hours, left axis for wind speed measured with reference anemometer GIOM 3000.

The blue signal consists from rectangular parts which concludes to existence of minimal value of time resolution. It is also proof of wind speed averaging. The sensitivity and time step resolution of developed sensor are clearly higher than in case of reference anemometer.

6 Final conclusion

After seeing the results it was quite easy to establish the measurement range. Considering sensor's saturation value 0,7au, the maximal speed of wind gust of developed sensor can be stated as 20m/s. Mechanical stress caused by sensor's bending transfers on the FBG grating[1], is strictly linear under the saturation value. The separation of thermal modulation from wind speed signal was achieved by adjusting the evaluating and processing algorithm. Considering equations in theoretical background,it is clearly an option to do just the opposite, which concludes to possibility of measuring the thermal changes in outside environment, neglecting the wind gust.

Any mechanical instability in sensor's construction was not observed a so far. Range of thermal stability is limited only by quality of used components. Sensor has no mechanically rotation parts in spite of used reference anemometers. The attributes of used components does not suggest any special temperature limits, so sensor is believed to work correctly in standard conditions from - 20°C up to +50°C. The maximal air speed the sensor has been exposed to was about 40m/s. This value is over the force of hurricane according to Beaufort wind force scale[2]. For purpose of protection of critical infrastructures are the results more then satisfactory.

The reproducibility of manufacturing process are disputable. A high dependency of rotation symmetry (circular function) on internal structure and the sequence of construction steps is indubitable from tests results. This inevitably makes any further handmade sensor partly original. The set of tests must be made to find the characteristic saturation value and establish the circular function for every single sensor. A different sets of material would have to be used, which would significantly raise the price of developed sensor for serial production (for which the sensor was not developed). The maximum outcome of manufacturing process (preserving the actual construction process) is stated to be in tens of pieces per year so far.

The dynamic range of use depends on proportions of used components. Its dependence can be seen in chapter 2 - theoretical background. The sensitivity of developed sensor is visible from last long-term tests in real environment. Sensor's resolution is under 0,5m/s, according to scale of reference signal from commercially available anemometer. Its precision depends on used data processing algorithm.

[1] Which is special diffraction structure used to cause a wavelength shift in characteristic spectral pattern of incoming light.

[2] Scale relates the wind speed to observed conditions at sea or on land.

7 Annexes

7.1 Used FBG

Figure 7.1: Annex 1 - Used FBG

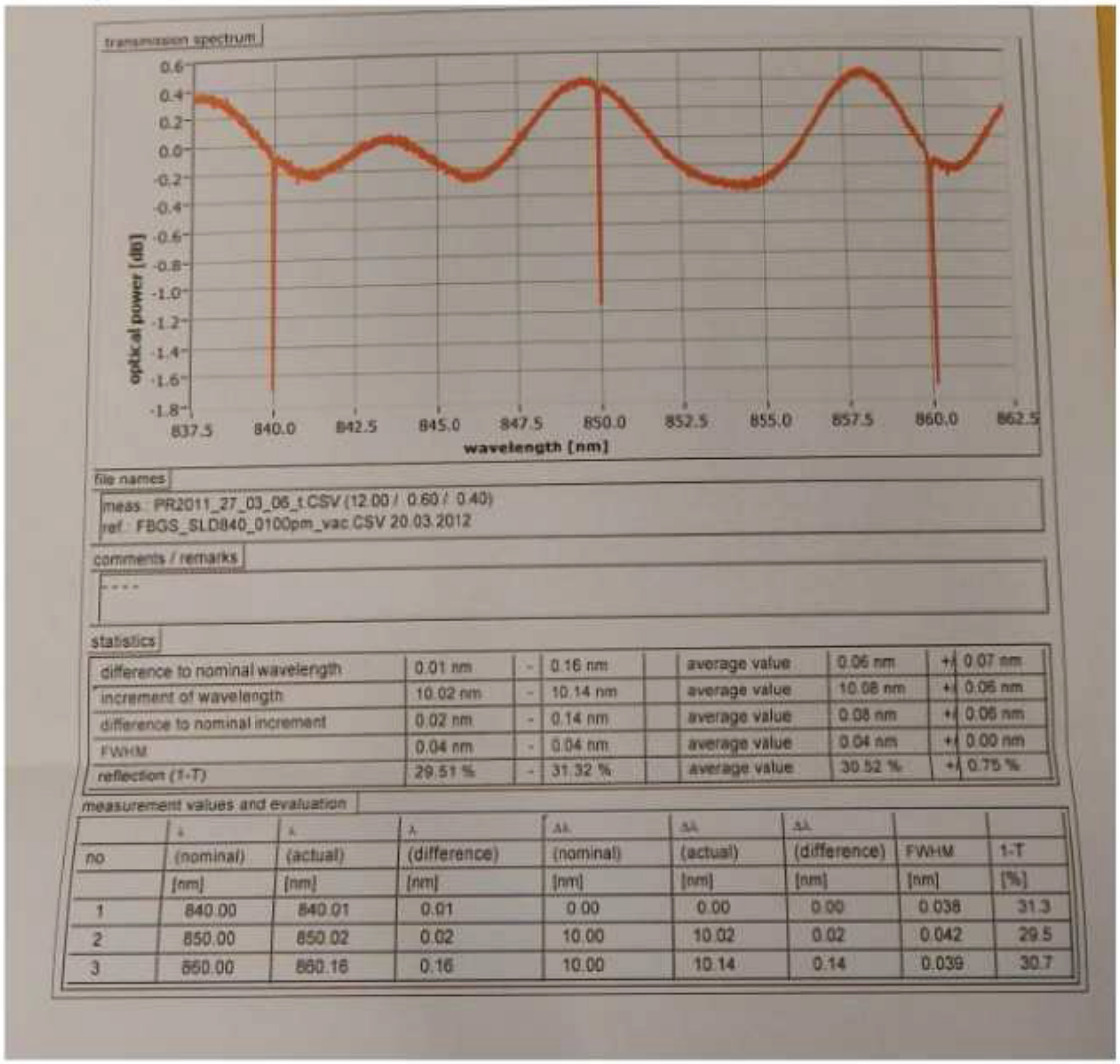

7.2 Clamping structure

Figure 7.2: Annex 2 - clamping structure

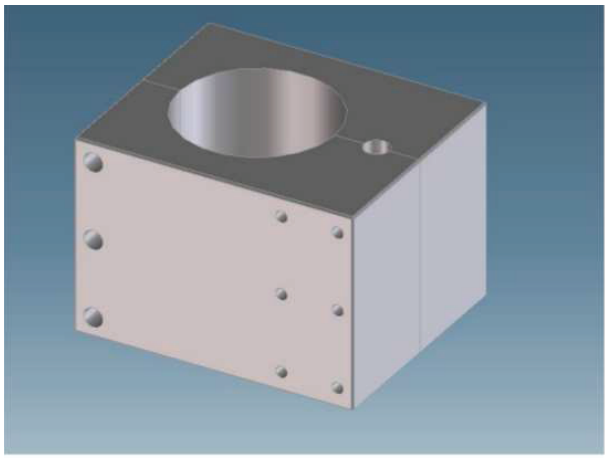

7.3 Dynamometer

Figure 7.3: Illustration picture of used dynamometer

7.4 Reference air-screw anemometer

Figure 7.4: Illustration picture of used air-screw reference anemometer

7.5 Tables of measured data

Rotation symmetry				
Angle [°]	Absolute distance		Force	
	Small coil	Big coil	0.5N	1N
0	0,6702	0,7101	0,1925	0,3556
5	0,6736	0,7116	0,1851	0,3867
10	0,6576	0,6978	0,1900	0,4131
15	0,6930	0,6870	0,2017	0,4093
20	0,6921	0,6734	0,1836	0,4264
25	0,6719	0,6552	0,1971	0,3882
30	0,6588	0,6370	0,1954	0,4021
35	0,6483	0,6190	0,1852	0,3253
40	0,6273	0,6110	0,1740	0,3713
45	0,6108	0,5980	0,1637	0,3714
50	0,5979	0,5858	0,1588	0,3628
55	0,5611	0,5691	0,1703	0,3629
60	0,5219	0,5488	0,1710	0,3473
65	0,5166	0,5263	0,1368	0,3031
70	0,4798	0,5119	0,1361	0,3063
75	0,4560	0,4880	0,1160	0,2911
80	0,4298	0,4590	0,1107	0,2806
85	0,4201	0,4411	0,1106	0,2677
90	0,3961	0,4181	0,0990	0,1918
95	0,3758	0,3979	0,0856	0,2550
100	0,3552	0,3826	0,0868	0,2166
105	0,3276	0,3586	0,0923	0,2204
110	0,3027	0,3408	0,0738	0,1974
115	0,3007	0,3208	0,0653	0,1707
120	0,2964	0,3026	0,0602	0,1685
125	0,2723	0,2776	0,0546	0,1652
130	0,2481	0,2716	0,0634	0,1559
135	0,2519	0,2557	0,0556	0,1370
140	0,2196	0,2503	0,0567	0,1330
145	0,2229	0,2442	0,0530	0,1192
150	0,2163	0,2278	0,0550	0,1129
155	0,2070	0,2148	0,0527	0,1158
160	0,1893	0,2262	0,0558	0,1111
165	0,1900	0,2183	0,0538	0,1029
170	0,1594	0,2154	0,0540	0,1058
175	0,1544	0,2152	0,0503	0,1020
180	0,1516	0,2304	0,0557	0,1088
185	0,1668	0,2464	0,0572	0,1006
190	0,1626	0,2479	0,0557	0,1028
195	0,1846	0,2707	0,0610	0,1243
200	0,1941	0,2766	0,0647	0,1179
205	0,2033	0,2833	0,0648	0,1482
210	0,2051	0,3017	0,0787	0,1462

Rotation symmetry				
Angle [°]	Absolute distance		Force	
	Small coil	Big coil	0.5N	1N
225	0,2699	0,3378	0,0700	0,1548
230	0,2924	0,3489	0,0767	0,1628
235	0,2995	0,3674	0,0930	0,1703
240	0,3210	0,3850	0,0868	0,2102
245	0,3045	0,4029	0,1053	0,2093
250	0,3681	0,4233	0,1223	0,2204
255	0,3711	0,4402	0,1172	0,2544
260	0,4014	0,4553	0,1297	0,2453
265	0,4047	0,4889	0,1304	0,2710
270	0,4156	0,5222	0,1404	0,2793
s275	0,4418	0,5238	0,1434	0,2911
280	0,4348	0,5474	0,1463	0,2907
285	0,5024	0,5679	0,1428	0,3016
290	0,4844	0,5871	0,1836	0,3174
295	0,4809	0,6018	0,1507	0,3201
300	0,5664	0,6137	0,1600	0,3616
305	0,5437	0,6324	0,1566	0,3393
310	0,5758	0,6428	0,1644	0,3694
315	0,5672	0,6537	0,1809	0,3814
320	0,6076	0,6857	0,1894	0,4010
325	0,6281	0,6906	0,1831	0,4068
330	0,6436	0,7093	0,2027	0,3874
335	0,6828	0,7073	0,2246	0,4228
340	0,6791	0,7170	0,2104	0,4232
345	0,6924	0,7169	0,2170	0,4202
350	0,6956	0,7123	0,2069	0,4319
355	0,6800	0,7078	0,2090	0,4236
Variation	1,40E-04	6,35E-05	1,32E-03	2,00E-05

Linearity - absolute distance				
Distance [cm]	0°	90°	180°	270°
1	0,0833	0,0595	0,0408	0,1244
2	0,1683	0,1168	0,0633	0,1856
3	0,2385	0,1715	0,0937	0,2423
4	0,2993	0,2163	0,1197	0,2822
5	0,3574	0,2587	0,1530	0,3287
6	0,4219	0,2978	0,1900	0,3756
7	0,5025	0,3399	0,2233	0,4256
8	0,5897	0,3836	0,2533	0,4798
9	0,6640	0,4437	0,2731	0,5313
10	0,7477	0,4830	0,3032	0,6031
11	0,8063	0,5403	0,3278	0,6640
12	0,8724	0,6004	0,3499	0,7256
13	0,9589	0,6572	0,3756	0,7670
Variation	2,50E-05	4,50E-06	2,54E-06	6,18E-06

Force linearity - without normalization				
F [N]	0°	90°	180°	270°
0,5	0,3631	0,2407	0,1894	0,3186
1	0,6244	0,3751	0,2725	0,4911
1,5	0,8104	0,5111	0,3478	0,6579
2	0,9439	0,6214	0,3810	0,7332
2,5	1,0014	0,6640	0,3946	0,7562
3	1,0512	0,6554	0,3844	0,7676
Variation	4,39E-05	1,41E-05	1,13E-05	1,67E-05

Force linearity - with normalization				
F [N]	0°	90°	180°	270°
0,5	0,3454	0,3626	0,4800	0,4150
1	0,5940	0,5649	0,6906	0,6398
1,5	0,7710	0,7697	0,8814	0,8571
2	0,8979	0,9359	0,9656	0,9553
2,5	0,9526	1,0000	1,0000	0,9852
3	1,0000	0,9871	0,9744	1,0000
Variation	4,39E-05	1,41E-05	1,13E-05	1,67E-05

Car roof - response test	
Speed [m/s]	Sensor response
5,1	0,0660
5,5	0,1333
6,2	0,0333
6,3	0,0467
7,7	0,1433
8,6	0,3000
8,7	0,0967
8,8	0,5897
9,6	0,2333
9,7	0,4533
12,7	0,5267
14,7	0,7927
15,6	0,8510
20,8	0,6593
25,0	0,6213
34,7	0,7513
40,0	0,6923
40,8	0,7000
45,0	0,7230
45,0	0,7393
50,0	0,7063

Bibliography

[1] PROLL, Guenther. R. Narayanaswamy, O.S. Wolfbeis (eds.): Optical Sensors. AnalyticOal and Bioanalytical Chemistry [online]. 2005, vol. 381, issue 1, s. 18-19 [cit. 2014-03-11]. DOI: 10.1007/s00216-004-2813-9.

[2] YUE, Yongzhe, Zhanmin ZHAO a Ran LI. Dual Optical Fiber Temperature Sensor Application in Mechanical Engineering. [online]. s. 91 [cit. 2014-03-11]. DOI: 10.1007/978-3-642-31507-7_16.

[3] Fiber Optic Sensors [online]. Hoboken, NJ, USA: John Wiley, 2011-07-11 [cit. 2014-03-11]. Dostupné z: http://link.springer.com/10.1007/978-3-642-31507-7_16

[4] ŠAŠEK, Ladislav a Jakub MARŠÁLEK. SAFIBRA S.R.O. ŘÍČANY. Zařízení pro identifikaci a měření nárazů a rychlosti tekutin, zejména větru [patent]. Czech Republic. 2013, 28277. Uděleno 02.01.2014. Zapsáno 19.12.2013. Dostupné z: http://isdv.upv.cz/portal/pls/portal/portlets.pts.det?xprim=2020035&lan=cs

[5] HILL, K.O. a MELTZ. Fiber Bragg grating technology fundamentals and overview. Journal of Lightwave Technology [online]. vol. 15, issue 8, s. 1263-1276 [cit. 2014-03-22]. DOI: 10.1109/50.618320. Dostupné z: http://ieeexplore.ieee.org/lpdocs/epic03/wrapper.htm?arnumber=618320

[6] FBGS DRAW TOWER GRATINGS. DTG® Technologies [online]. 2014 [cit. 2014-03-22]. Dostupné z: http://www.fbgs.com/technology/dtg-technology/

[7] FBGS DRAW TOWER GRATINGS. DTG® Advantages [online]. 2014 [cit. 2014-03-22]. Dostupné z: http://www.fbgs.com/technology/advantages-dtgs/

[8] BAUMEISTER, Philip. Optical coating technology. Bellingham, WA.: SPIE Optical Engineering Press, 2004, 1 v. (various pagings). ISBN 08-194-5313-7.

[9] FOCENTER, Fiber Optic Center INC. FC/APC conncetors and Adapters: Product Data Sheet. www.focenter.com [online]. New Bedford, MA USA: 23 Centre Street, 2014 [cit. 2014-03-22]. Dostupné z: http://www.focenter.com/Fiber%20Optic%20Center%5CMolex%5CData%20Sheets%5CPDFs%5CFC%20APC%20Connectors%20and%20Adapters.pdf

[10] PRINCETEL, INC. Corning SMF-28e Optical Fiber: Product Information. Corning, NY 14831 USA, 2007, 4 s. Dostupné z: http://www.princten.com/datasheets/smf28e.pdf

[11] GRAHAM-SMITH, Francis, Terry A KING a Dan WILKINS. Optics and photonics: an introduction. 2nd ed. Hoboken, NJ: J. Wiley, c2007, x, 506 p., [8] p. of plates. ISBN 978-047-0017-845.

[12] SPARROW, I. J. (2005) Development and applications of UV written waveguides. University of Southampton, Faculty of Engineering and Applied Science, Optoelectronic Research Centre, Doctoral Thesis . [cit. 2014-03-22], Online at: http://www.orc.soton.ac.uk/viewpublication.html?pid=3539

[13] FIALA, Pavel a Ivan RICHTER. Fyzikální optika. Vyd 2., přeprac. Praha, 2005. 208 s. ISBN 80-010-3183-7.

[14] SCHWARTZ, Mel. Encyklopedia of Smart Materials. Volume 2 M-Z online. New York: John Wiley, 2002 [cit. 2014-03-29]. ISSN 978-0-471-17780-7.

[15] FBGs technology. FBGS INTERNATIONAL NV. FBGS TECHNOLOGIES GMBH. FBGS - Draw Tower Gratings: Principle of Fiber bragg grating [online]. 2014 [cit. 2014-03-29]. Dostupné z: http://www.fbgs.com/website/fbgs/assets/images/FBG_principle_1.jpg

[16] CARTY, Joseph James. Resistance Coefficients for orbs on Plane Boundary. Massachusetts, USA, 1957. Dostupné z: http://dspace.mit.edu/bitstream/handle/1721.1/12152/31990887.pdf. B.S. Thesis. M.I.T.

[17] KING, R.P. Introduction to practical fluid flow. [Online-Ausg.]. Oxford, 2002. ISBN 07-506-4885-6.

[18] NOŽIČKA, Jiří. Mechanika tekutin. Vyd. 1. Praha: Vydavatelství ČVUT, 2002, 165 s. ISBN 80-010-2865-8.

[19] LINHART, Jiří. Mechanika tekutin. 2. vyd. Plzeň: Západočeská univerzita v Plzni, 2009, 123 s. ISBN 978-80-7043-766-7.

[20] MRAD, Nezih. Optical Fiber Sensing Technology: Introduction and evaluation and application. Encyclopedia of smart materials [online]. 2002, s. 39 [cit. 2014-05-02].

[21] GUAN, Bai-Ou, Hwa-Yaw TAM, Siu-Lau HO, Weng-Heng CHUNG a Xiao-Yi DONG. Simultaneous strain and temperature measurement using a single fibre Bragg grating. Electronics Letters [online]. Překlad John Bester. 2000, vol. 36, issue 12, s. 1018- [cit. 2014-05-02]. DOI: 10.1049/el:20000754. Dostupné z: http://digital-library.theiet.org/content/journals/10.1049/el_20000754

[22] Mechanika - Ohyb: Ohyb vetknutého nosníku. In: Http://physics.mff.cuni.cz/kfpp/: Katedra fyziky povrchů a plazmazu [online]. [cit. 2014-05-16]. Dostupné z: http://physics.mff.cuni.cz/kfpp/skripta/kurz_fyziky_pro_DS /display.php/kontinuum/3_5